
Since January 2020 Elsevier has created a COVID-19 resource centre with free information in English and Mandarin on the novel coronavirus COVID-19. The COVID-19 resource centre is hosted on Elsevier Connect, the company's public news and information website.

Journal of Molecular Structure 1245 (2021) 131020

Contents lists available at ScienceDirect

Journal of Molecular Structure

journal homepage: www.elsevier.com/locate/molstr

# Novel piperazine based compounds as potential inhibitors for SARS-CoV-2 Protease Enzyme: Synthesis and molecular docking study

Alaa Z. Omar[a,*], Tawfik M. Mosa[a], Samer K. El-sadany[a], Ezzat A. Hamed[a], Mohamed El-atawy[a,b]

[a] Chemistry Department, Faculty of Science, Alexandria University, P.O. 426 Ibrahemia, Alexandria 21321, Egypt
[b] Chemistry Department, Faculty of Science, Taibah University, Yanbu 46423 Saudi Arabia

ARTICLE INFO

*Article history:*
Received 19 February 2021
Revised 9 June 2021
Accepted 30 June 2021
Available online 4 July 2021

*Keywords:*
COVID-19
Protease enzyme inhibitors
SARS-CoV-2
Piperazine
Mannich reaction

ABSTRACT

Structurally diverse piperazine-based compounds hybrid with thiadiazole, isatin or with sulfur/nitrogen, functionalities were synthesized. The structures of the new compounds were established based on their spectral data and elemental analysis. The physicochemical, bioactivity scores and pharmacokinetic behavior of all the prepared ligands were evaluated using *in silico* computational tools. The new piperazine ligands have been screened for their inhibition activity against SARS-CoV-2 protease enzyme using molecular docking analysis. The docking studies showed that all the ligands have been docked with negative dock energy onto the target protease protein. Moreover, Molecular interaction studies revealed that SARS-CoV-2 protease enzyme had strong hydrogen bonding interactions with piperazine ligands. The present *in silico* study thus, provided some guidance to facilitate drug design targeting the SARS-CoV-2 main protease.



## 1. Introduction

In December 2019, the seventh strain of Human coronaviruses has begun in the animal and seafood market in Wuhan, China, and rapidly identified as a novel beta coronavirus, Patients initially infected with this virus suffered severe respiratory tract infections, pneumonia illness, and fever [1-4]. WHO (World Health Organization) characterized the virus disease as COVID-19 (coronavirus disease-2019). Recently, WHO changed the name of the virus to be SARS-CoV-2 (severe acute respiratory syndrome-coronavirus-2) [5-7] instead of (2019-nCoV) that's due to the high similarity of the nucleotide sequence with SARS-CoV and MERS-CoV. In March 2020, SARS-CoV-2 rapidly spread worldwide in more than 100 countries and WHO officially declared COVID-19 as pandemic or global infectious disease [8,9]. In 10th of September 2020 the number of COVID-19 infected people patients reached more than 28,021,800 people all over the world out of which ≈ 20,099,000 patients have been recovered and ≈908,000 death [10]. The number of infected people is still growing rapidly which make the finding of anti-SARS-CoV-2 drug become an essential and a challenge for scientists.

SARS-CoV-2 are positive sense single-stranded RNA virus, long about 30,000 bp, employs host cellular components to achieve its physiological activities such as protein synthesis and replication, subsequently accomplishes pathological damage to the host cells although some probable drugs are under investigation worldwide [11-15]. The severity of SARS-CoV-2 requires an urgency to develop a vaccine, which is an expensive and time-consuming process. However, nowadays different ligand-based computational techniques and structure-based modeling techniques could be fruitful approach to design novel inhibitors against SARS-CoV-2 [16,17].

Several significant targets have been documented to participate in the biological events critical to SARS-CoV replication, one of these targets is the main protease (Mpro)/chymotrypsin-like protease (3CLpro) [18-22], It have been successfully crystallized from COVID-19, structured and repositioned in the Protein Data Bank (PDB) and is reachable by the public. This protease represents a potential target for the inhibition of CoV replication [12,23].

Piperazine scaffolds exist in several different biologically active compounds including some antiviral agents such as Delavirdine and Indinavir, Fig. 1, which are commonly used to treat human immunodeficiency virus (HIV) [24-27]. The previously reported antiviral activity of piperazine-based drugs encouraged us to design a variety of ligands containing piperazine moiety along with other functionalities or other heterocyclic rings in order to make screening of large library of piperazine based drugs to evaluate their inhibition against SARS-CoV-2 and to identify new active compounds

* Corresponding author.
*E-mail addresses:* Alaazaki@alexu.edu.eg (A.Z. Omar), mohamed.elatawi@alexu.edu.eg (M. El-atawy).

https://doi.org/10.1016/j.molstruc.2021.131020
0022-2860/

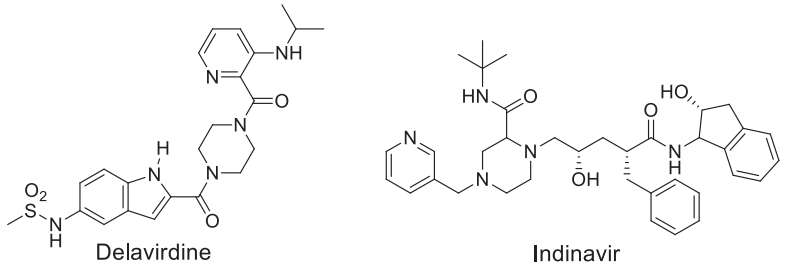


**Fig. 1.** Examples for antiviral drugs containing piperazine moiety.

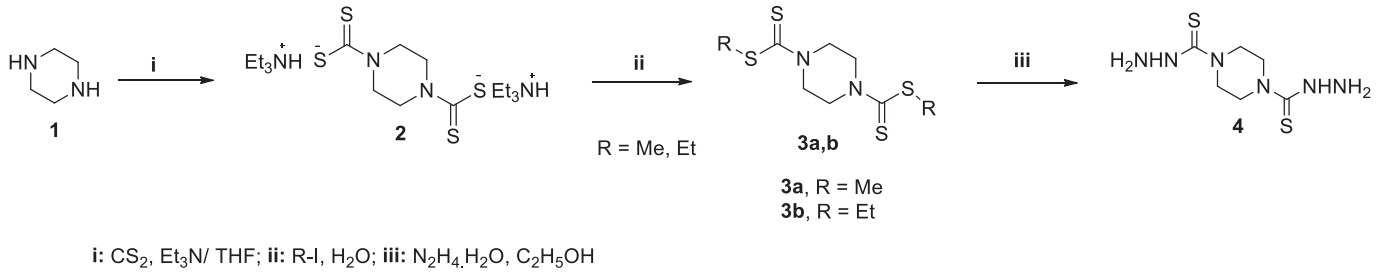


**Scheme 1.** Synthesis of symmetrical *N,N′*-disubstituted piperazines.

using high throughput technique. Herein we report our results on synthesis of several compounds containing piperazine ring hybrid with other heterocyclic rings or with sulfur or nitrogen functionalities followed by finding the binding modes of synthesized ligands with SARS-CoV-2 main protease using docking studies. The aim of the present research is focused on the use of computational techniques and structure-based modeling techniques for some synthesized piperazine-based compounds as possible inhibitors against SARS-CoV-2. Thus, this study is an initiative to facilitate development of antiviral drug discovery model that could help to pave the way to the worldwide efforts to combat SARS-CoV-2.

## 2. Results and discussion

### 2.1. Chemistry

Multiple functionalization of piperazine at 1 and/or 4 positions were synthesized owing to the biological and pharmacological activities of piperazine derivatives. The nucleophilic character of piperazine at these positions promote a variety of substitution reactions which allow the existence of hydrophobic and hydrophilic parts necessary to bind through different electrostatic and hydrogen bonding interactions. The synthetic route for the target piperazine based compounds **2–11** is simple, straight forward and illustrated in Schemes 1-4. The structures of the synthesized compounds were confirmed by their IR, $^1$H NMR, $^{13}$C NMR and elemental analysis.

Piperazine bis-thiosemicarbazide **4** was prepared via multistep reaction involved nucleophilic addition of carbon disulfide to piperazine **1** in presence of triethyl amine, producing intermediate salt **2** [28]. That subjected to S-alkylation reaction using alkyl halide to afford bis(carbo-dithioate) **3** which on subsequent treatment with hydrazine hydrate afforded the desired target compound **4**, Scheme 1.

It has been reported that 1,3,4-thiadiazole nucleus has the ability to form mesoionic systems associated with discrete regions of negative and positive charges [29,30]. Furthermore, it gave the associated compounds high lipophilicity which allow their effective cross of cellular membranes [31], leading to good oral absorption and strong interactions with biomolecules (e.g., proteins, nucleic acids, etc.) [32]. Accordingly, the bis thiosemicarbazide **4** has been used as a precursor for building up thiadiazole-piperazine hybrid compounds **5–7.**

The treatment of compound **4** with carbon disulfide ($CS_2$) in boiling DMF led to the formation of 5,5′-(piperazin-1,4-diyl)bis(1,3,4-thiadiazole-2-thiol) **5** through additive cyclization process. Subsequent thiol-alkylation of product **5** using either methyl or ethyl iodide in the presence of ethanolic potassium hydroxide afforded S-methyl alkylated product **6a** or S-ethyl alkylated product **6b,** respectively. Further oxidation of **6a** using ethanolic hydrogen peroxide produced the corresponding sulphone **7**. Moreover, the Condensation of **4** with 4-nitrobenzaldehyde in presence of acetic acid has given 1,4-bis(4-nitrobenzylidene)piperazine-1,4-bis(carbothiohydrazide) **8,** Scheme 2**.**

The FTIR analysis of the bis-dithiocarbamate **3a, 3b** showed bands at 1458 and 1463 cm$^{-1}$ that can be ascribed to the vibration characteristic for dithiocarbamate group (NCSS). The peaks observed at 2913 cm$^{-1}$ and 2992 cm$^{-1}$ are respectively related to the symmetric and asymmetric stretching vibrational of C–H of alkyl groups. Moreover, proton NMR (DMSO–$d_6$) of compound **3a** revealed two singlets at $\delta$ 4.16 and 2.67 ppm due to methylene groups of piperazine and methyl groups, respectively. Whereas, ethyl groups of **3b** revealed a quartet and triplet signals in $^1$H NMR at $\delta$ 3.23 and 1.26 ppm, respectively. The infrared spectrum of **4** exhibited bands in the region 3267–3088 cm$^{-1}$ corresponding to the absorption characteristic for N–H stretching. Moreover, $^1$H NMR (DMSO–*d6*) of **4** revealed broad $D_2O$-exchangeable singlets at $\delta$ 9.07 and 4.87 ppm attributed to the existence of hydrazino group. Furthermore, $^{13}$C NMR spectrum of **3a, 3b** and **4** exhibited signals at $\delta$ 199, 195 and 182 ppm respective to their thiocarbonyl carbon, respectively. The $^1$H NMR (DMSO–*d6*) spectrum of **5** exhibited a broad exchangeable-signal corresponding to protons of thiol groups. Moreover, methyl protons of **6a** and **7** revealed signals in proton NMR at $\delta$ 2.68 and 3.04 ppm, respectively. The ethyl group of **6b** was also displayed in $^1$H NMR as a quartet and a triplet at $\delta$ 3.17 and 1.41 ppm. Additionally, $^{13}$C NMR spectra of **5–7** showed two quaternary carbons in region 128.27–184.46 ppm corresponding to thiadiazole ring. Compound **8** showed the characteristic infrared absorption bands for $NO_2$ stretching at 1519 and 1344 cm$^{-1}$. Furthermore, $^1$H NMR spectrum of **8** exhibited singlet at $\delta$ 8.86 ppm for azomethine proton (*N*=CH). $^{13}$C NMR spectrum of **8** showed two quaternary carbons corresponding to its phenyl rings.

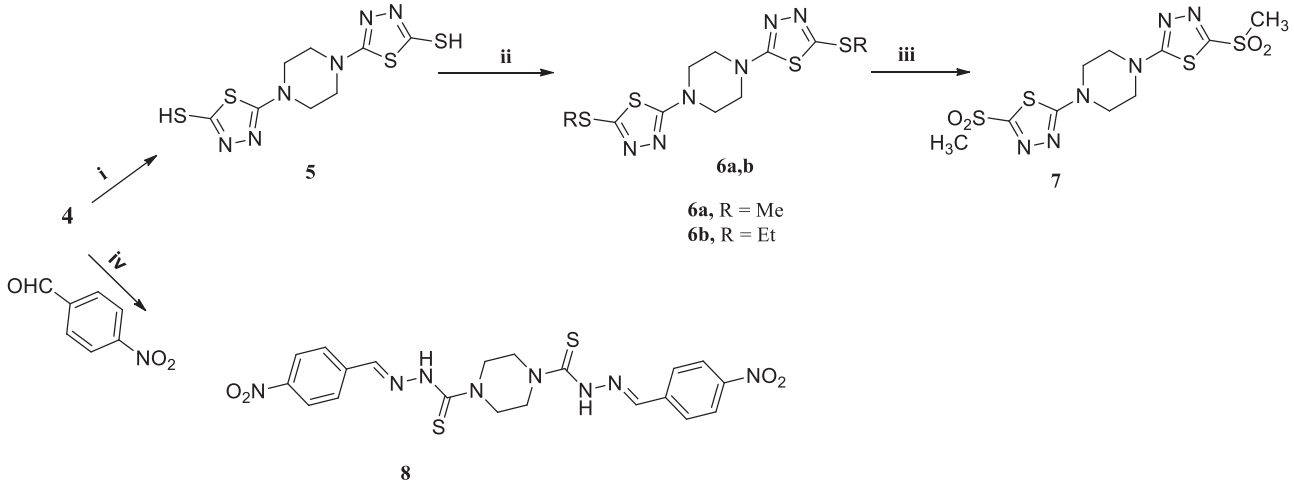


**i:** $CS_2$, DMF; ii: R-I, KOH/$H_2O$, $C_2H_5OH$; **iii:** $H_2O_2$, $C_2H_5OH$; **iv**: AcOH

**Scheme 2.** Synthesis of piperazine hybrid with bis(1,2,4-thiadiazole) moiety.

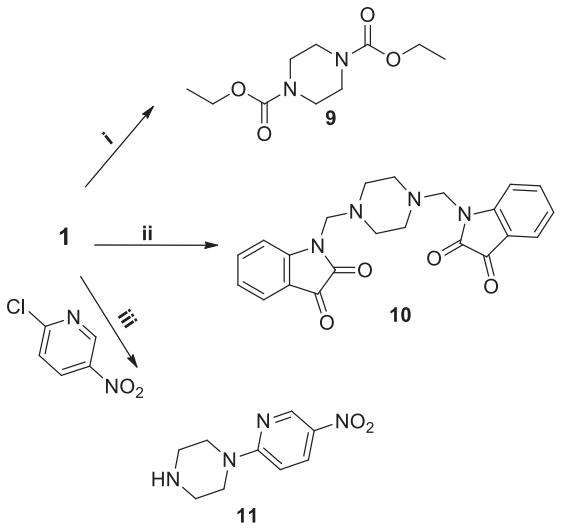


**i:** $ClCO_2C_2H_5$, $C_2H_5OH$; **ii:** Isatin / HCHO, $C_2H_5OH$; **iii:** NaH / Dioxane

**Scheme 3.** Synthesis of piperazine derivatives **9–11**.

The good antiviral activity of *N*-substituted isatin grabbed our attention to link isatin to piperazine [33-36]. Accordingly, bis-Mannich base **10**, which represent piperazine-isatin hybrid compound was prepared by Aminomethylation of isatin via Mannich reaction using piperazine **1** as secondary amine and formaldehyde at room temperature. Furthermore, piperazine **1** has been transformed into diethyl piperazine-1,4-dicarboxylate **9** by stirring with ethyl chloroformate in dichloromethane at 0 °C followed by addition of triethylamine, Scheme 3. This because carbamates have been known as a peptide bond surrogate in medicinal chemistry [37], due to their ability to permeate cell membranes and chemical stability.

The infrared spectrum of the bis-dicarbamate **9** showed absorption band at 1708 $cm^{-1}$ corresponding to the stretching vibration of carbamate group. The $^1H$ NMR spectrum of **9** exhibited a quartet and triplet at 4.13 and 1.24 ppm for the ethyl protons. The carbonyl carbon of **9** was displayed also in $^{13}C$ NMR at 155.37 ppm. The infrared spectrum of the bis-Mannich base **10** revealed two sharp absorption bands at 1738 and 1612 $cm^{-1}$ attributable to the vibration of ketonic and amidic carbonyls in isatin moiety, respectively. $^1H$ NMR spectrum of **10** showed a singlet at $\delta$ 4.38 ppm corresponding to the protons of the methylene's spacer. Moreover, $^{13}C$ NMR spectrum of **10** exhibited two signals at $\delta$ 183.20 and 158.99 can be ascribed to carbonyl carbons of isatin moiety and a signal at 61.53 for carbon of the methylene spacer.

As an extension to the present investigation, mono substituted piperazine has been synthesized either by direct replacement reaction of equimolar amounts of piperazine and active aryl halide or by amination\ cyclization of bis(2-chloroethyl)amine. In this way, pyridyl piperazine **11** has been synthesized by reaction of piperazine **1** and 2–chloro-5-nitropyridine in presence of sodium hydride in 1,4-dioxane, Scheme 3**.** Moreover, phenyl piperazine **12** has been prepared by refluxing bis(2-chloroethyl)amine hydrochloride with *p*-bromoaniline in presence of *n*-propanol and potassium carbonate. The bis(2-chloroethyl)amine has been produced by chlorination of the commercially available diethanolamine using thionyl chloride [38],Scheme 4.

The infrared spectrum of **11** and **12** showed absorption characteristic for N–H stretching in the region 3404–3340 $cm^{-1}$. The asymmetric structure of **11** and **12** has been verified through NMR spectroscopic data. Accordingly, due to the molecular asymmetry of **11** and **12** their piperazine moiety showed two peaks in both proton and $^{13}C$ NMR.

### 2.2. Physicochemical properties [39-41]

The physicochemical and biochemical properties of all the candidate ligands **3–12** were evaluated by using *in silico* computational tools**.** The oral bioavailability of a drug candidate can be predicted via Lipinski rule of five (RO5). This rule is based on physicochemical parameters of the tested ligands, including: Molecular weight (MW) not greater than 500 g/mol; A partition coefficient clogP less than or equal five; number of hydrogen bond donors (HBD) (NH and OH groups) not greater than five; and number of hydrogen bond acceptors (HBA) (O and N atoms) not exceeds ten. The synthesized ligands **3–12** were validated through descriptors of Lipinski's rule of five (RO5 analysis). Results, Table 1, interestingly showed that nine of the tested ligands namely, **3a, 3b, 5, 6, 7, 9, 10, 11**, and **12** were fully in agreement to Lipinski's rule of five. Ligand **4** exhibited single violation regarding hydrogen donor as well as ligand **8** showed two violations regarding hydrogen acceptor and molecular weight. Another useful predication for oral bioavailability is computation of Veber descriptors namely, num-

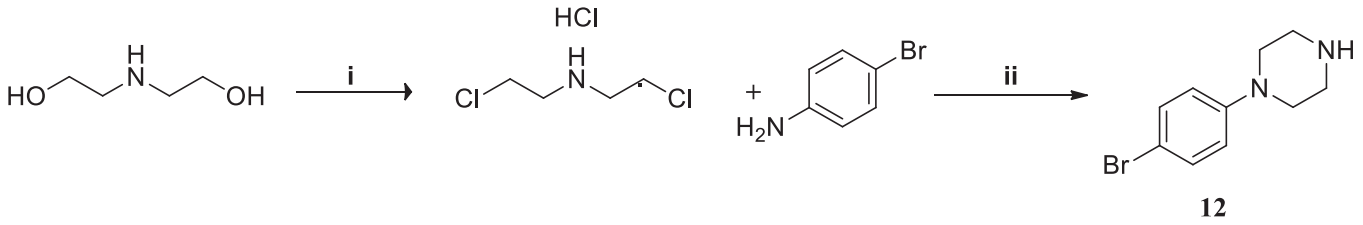


**Scheme 4.** Synthesis of 1-(4-bromophenyl)piperazine **12**.

**Table 1**
Predicted physicochemical properties for ligands **3–11**.

| Lig. | Mwt | Log P | H-DON | H-ACC | Violation | TPSA | NROTB | Molcular flexibility | Drug like test | Polar volume | volume | Drug Likeness |
|---|---|---|---|---|---|---|---|---|---|---|---|---|
| **3a** | 266.00 | 2.48 | 0 | 2 | 0 | 6.22 | 4 | 8.17 | 1 | 32.87 | 247.50 | −0.99 |
| **3b** | 294.03 | 3.25 | 0 | 2 | 0 | 6.22 | 6 | 9.93 | 1 | 38.875 | 285.01 | −0.92 |
| **4** | 234.07 | −1.19 | 6 | 6 | 1 | 73.47 | 4 | 4.44 | 1 | 242.75 | 228.27 | −0.24 |
| **5** | 317.98 | 0.90 | 0 | 6 | 0 | 51.18 | 2 | 4.71 | 1 | 78.25 | 230.05 | −0.72 |
| **6a** | 346.01 | 2.98 | 0 | 6 | 0 | 52.31 | 4 | 5.89 | 1 | 55.62 | 270.65 | −0.71 |
| **6b** | 374.04 | 3.70 | 0 | 6 | 0 | 52.31 | 6 | 7.16 | 1 | 57.625 | 308.68 | −0.61 |
| **7** | 409.99 | −0.40 | 0 | 10 | 0 | 112.63 | 4 | 6.13 | 1 | 70.75 | 310.26 | −0.34 |
| **8** | 500.10 | 1.91 | 2 | 12 | 2 | 122.81 | 10 | 6.82 | 0 | 150.25 | 466.96 | −0.17 |
| **9** | 230.12 | 1.27 | 0 | 6 | 0 | 45.99 | 6 | 4.35 | 1 | 18 | 247.05 | −0.96 |
| **10** | 404.14 | 1.14 | 0 | 8 | 0 | 68.12 | 4 | 3.34 | 1 | 72.25 | 431.14 | 0.62 |
| **11** | 208.09 | 0.15 | 1 | 6 | 0 | 62.51 | 2 | 2.23 | 1 | 70.5 | 186.72 | −0.90 |
| **12** | 240.02 | 2.31 | 1 | 2 | 0 | 15.65 | 1 | 3.01 | 1 | 51.75 | 188.20 | −1.62 |

ber of rotatable bonds NROTB and topological polar surface area TPSA. Rotatable bonds are defined as any single bond, not in a ring, bound to a nonterminal heavy atom. Excluded from the count are amide C–N bonds because of their high rotational energy barrier. The NROTB is a measure for the molecular flexibility, furthermore, for good oral bioavailability NROTB shouldn't exceed than 10**.** All ligands **3–12** exhibited ten or fewer rotatable bonds. Additionally, TPSA can be defined as the surface area occupied by oxygen and nitrogen atoms and the polar hydrogens bonded to them and it is strongly reflective of polarity and hydrogen bonding capacity. TPSA is a good descriptor characterizing drug absorption including bioavailability, blood-brain barrier penetration and intestinal absorption, predicted TPSA values of all ligands **3–12** were less than 140 $A^2$ which is in accordance to the value known for most drugs which predict promising oral bioavailability. Furthermore, drug-likeness score was also computed as a collective descriptor of pharmacodynamic, pharmacokinetic and physicochemical properties of the tested ligands such as molecule size, electronic distribution, hydrogen bonding characteristics, hydrophobicity, and flexibility. Compounds with positive values of drug likeness are more probable to be drug-like. As illustrated, Table 1, only ligand **10** displayed positive score representing a promising drug-like behavior.

### 2.3. ***Prediction of bioactivity scores*** *[42-44]*

Encouraged by the good physicochemical properties of the ligands under study we extend the calculation of drug likeness score towards G protein-coupled receptors (GPCR), ion channel modulators (ICM), kinase inhibitors (KI), nuclear receptor ligands (NRL), protease inhibitors (PI) and other enzyme (EI) targets. Calculations have been done using Molinspiration software, Table 2. As a rule, a compound having bioactivity score with positive value (>0.00) is most probable to possess considerable biological activities, while values 0.00 to −0.50 are expected to be moderately active and if score is less than −0.50 it is assumed to be inactive. The predicted bioactivity scores of all synthesized ligands showed moderate activity against EI which indicate efficient binding to enzymes. Moreover, the results of the present study demonstrated that ligands **9** and **11** showed good bioactivity score (0.04 and 0.12, respectively) towards ICM, while ligands **8, 10** and **12** exhibited moderate bioactivities to ICM. Furthermore, ligands **7–10** displayed moderate bioactivity towards PI. Similar behavior has been shown by ligands **7–11** and ligands **8–11** with respect to KI and GPCR respectively. Additionally, moderate bioactivity scores toward the target NRL has been predicted for ligands **7, 9** only.

**Table 2**
Assessment of bioactivity scores for ligands **3–12** using Molinspiration software.

| Lig. | GPCR | ICM | KI | NRL | PI | EI |
|---|---|---|---|---|---|---|
| **3a** | −0.62 | −0.93 | −1.52 | −1.52 | −1.20 | −0.46 |
| **3b** | −0.67 | −0.92 | −1.41 | −1.33 | −1.05 | −0.45 |
| **4** | −1.06 | −0.9 | −1.00 | −1.62 | −1.10 | −0.45 |
| **5** | −0.86 | −0.73 | −0.57 | −1.04 | −0.54 | −0.16 |
| **6a** | −0.74 | −0.68 | −0.56 | −0.72 | −0.70 | −0.30 |
| **6b** | −0.65 | −0.63 | −0.65 | −0.67 | −0.58 | −0.35 |
| **7** | −0.54 | −0.66 | −0.39 | −0.48 | −0.36 | −0.20 |
| **8** | −0.47 | −0.44 | −0.48 | −0.58 | −0.50 | −0.29 |
| **9** | −0.19 | 0.04 | −0.44 | −0.38 | −0.20 | −0.12 |
| **10** | −0.18 | −0.45 | −0.14 | −0.58 | −0.2 | −0.03 |
| **11** | −0.34 | 0.12 | −0.25 | −0.90 | −0.62 | −0.20 |
| **12** | −0.64 | −0.20 | −0.61 | −1.14 | −0.96 | −0.51 |

### 2.4. *Pharmacokinetics and toxicity*

To assess the opportunity of future therapeutic application of the synthesized ligands, pharmacokinetic [45-47] behavior via ADME properties (absorption, distribution, metabolism and excretion) have been predicted *in silico* using pkCSM tool, Table 3. Regards to the predicted absorption, the obtained data revealed that all ligands **3–12** exhibited favorable human intestinal absorption (61–100%abs) where molecules with an absorbance less than 30% are poorly absorbed and not suitable for oral administration. Moreover, it was found that ligands displayed reasonable predicted water solubility except for ligands **7** and **9–12**. Furthermore, the skin permeability predicted values indicate that all of the ligands are likely skin permeable except for ligands **3b** and **12** which have skin permeability constant log kp greater than −2.5 cm/h. Con-

**Table 3**
In silico predicted pharmacokinetic properties of ligands **3–12** using pkCSM tool.

| | Absorption | | | Distribution | | Metabolism | | | Excretion | Toxicity | | | | |
|---|---|---|---|---|---|---|---|---|---|---|---|---|---|---|
| Lig. | S | IS | SP | BBBP | CNSP | CYP1A2 | CYP2C19 | CYP2C9 | TC | MTD | AMES | ORAT | HT | SS |
| **3a** | −3.45 | 91.88 | −2.59 | 0.39 | −3.36 | No | No | No | 0.53 | 0.57 | No | 3.03 | Yes | Yes |
| **3b** | −4.18 | 91.04 | −2.42 | 0.57 | −3.06 | Yes | Yes | No | 0.51 | 0.44 | No | 3.16 | No | Yes |
| **4** | −3.14 | 62.84 | −3.24 | −0.87 | −3.69 | No | No | No | −0.21 | 1.37 | No | 3.33 | No | Yes |
| **5** | −4.40 | 100.0 | −2.94 | −0.32 | −3.22 | Yes | No | No | 0.20 | 0.28 | No | 2.64 | Yes | No |
| **6a** | −4.50 | 95.77 | −2.90 | 0.05 | −3.13 | Yes | No | No | 0.29 | 0.17 | No | 3.19 | Yes | No |
| **6b** | −4.88 | 94.74 | −2.96 | 0.01 | −3.10 | Yes | No | No | 0.33 | 0.19 | No | 3.09 | Yes | No |
| **7** | −2.86 | 54.77 | −2.73 | −2.08 | −3.40 | No | No | No | 0.24 | 0.65 | No | 2.96 | Yes | No |
| **8** | −4.72 | 66.53 | −2.74 | −1.05 | −2.67 | No | No | No | −0.09 | −0.46 | Yes | 2.57 | Yes | No |
| **9** | −1.97 | 90.46 | −4.07 | −0.23 | −3.08 | No | No | No | 0.67 | 0.72 | No | 2.65 | No | No |
| **10** | −2.97 | 61.70 | −2.90 | −0.33 | −2.73 | No | No | No | 1.09 | −0.58 | No | 2.65 | Yes | No |
| **11** | −1.93 | 90.71 | −2.93 | −0.45 | −2.97 | No | No | No | 0.48 | 0.23 | Yes | 2.53 | Yes | No |
| **12** | −1.96 | 92.70 | −1.86 | 0.627 | −2.27 | Yes | No | Yes | 0.82 | 0.13 | No | 2.78 | Yes | Yes |

cerning blood brain permeability, the ability of the drug to cross into the brain is important to decrease toxicities and side effects. The predicted data revealed that ligands are lipophilic enough to cross the blood brain barrier except for ligand **7** which exhibited log BB less than −1. Additionally, most of the ligands having no permeation to central nervous system (CNS) with blood brain permeability-surface area product logPS less than −3. Regards to the predicted Metabolism properties, it was found that the ligands under study were predicted as inhibitors or non-inhibitors for some cytochrome P450 isoenzymes such as CYP1A2, CYP2C19 and CYP2C9. None of the assessed ligands was predicted as inhibitor for CYP2C19 or CYP2C9 except ligands **3b** and **12,** respectively. On the other hand, ligands **3b, 5, 6a, 6b** and **12** were predicted as CYP1A2 inhibitor. This inhibitory effect on CYP isoenzyme activity may cause the probability of drug interactions. Moreover, excretion properties expressed in total clearance log(CLtot) have been predicated for all ligands under study which is important for determining dosing rates to reach steady state concentrations.

The parameters related to toxicity including maximum tolerated dose (MTD), AMES test, oral rat acute toxicity (ORAT), hepatotoxicity (HT), and skin sensitization (SS) have been predicted. AMES test is employed to assess whether the drug is mutagenic or not [48]. All the synthesized ligands except **8** and **11** exhibited negative AMES tests indicating that they are non-mutagenic. Moreover, ligands showed relatively high predicted lethal dose value LD50 (2.53–3.33 mol/Kg) which is indicative of low acute toxicity.

The predicted hepatotoxicity showed that ligands **3a, 5, 6, 7, 8, 10, 11** and **12** would probably show hepatotoxicity associated with disrupted normal function of liver. However, most of the assessed ligands don't show skin sensitization

### 2.5. Molecular docking

Considering the global threat posed by COVID-19, and with no proven antiviral agent available for immediate relief, the current *in silico* study provide structural insights about the protease of SARS-CoV-2 and its molecular interactions with synthesized ligands **3–12** as protease inhibitors. Protease enzyme is essential for viral replication because it catalyzes the proteolytic process for the polyproteins that are translated from the viral RNA [49]. Thus, inhibition of the protease activity would block viral replication and unlikely to be toxic for human, which make protease one of the best drug discovery targets in case of coronaviruses. The activity of protease enzyme is blocked by binding of inhibitor molecules to the active site of the enzyme. Moreover, protease is suitable for designing wide-spectrum inhibitors because it contains large number of amino acids. All the eleven protease inhibitors candidates got docked onto the predicted 3D model of protease of SARS-CoV-2 with a negative dock energy value as shown in Table 4. Molecular interaction studies, Fig. 2, showed that protease model of SARS-CoV-2 had Asn142, Gly143, His163, Ser144, Met165, Glu166, Gln189, Thr26, His41, Thr25, Cys145, Phe140, Met49 and Arg188'' as the potential drug binding sites, with more than one drug binding site identified with eight inhibitors candidates. While for other ligands the structure had only one active site residue each. The best noted binding energy value was obtained for ligand **8** (−6.87 kcal/mol). This ligand exhibited hydrogen bonding interactions between its thiosemicarbazide moiety and three amino acids residue at the backbone of the enzyme namely, GLY143, ASN142 and THR26, as well as hydrogen bonding interaction between its nitro group and GLN189 residue. Moreover, ligand **10** with slightly lower protease inhibitory activity than **8** (binding energy ≈ −6.81), interacted with the active site at HIS43 and THR25 via H-p interactions and hydrogen bonding interactions through its isatin keto group and HIS163. Alternatively, ligand **12**, which showed the lowest protease inhibition among the nominated ligands, only displayed p-H binding interaction with the active site at MET165 via its phenyl rings but failed to display any hydrogen bonding interactions. It could be concluded that the appropriate substitution of the amino groups of the piperazine scaffold (ligands **8, 10, 6a, 6b** and **7**), showed significant hydrogen bonding interactions with SARS-CoV-2 protease enzyme that possibly allowed improved inhibitory activity. Based on the lowest dock energy value scored by **8** in relation to other ligands, this appears to be the drug of choice for treating COVID-19 infection. Since all the ligands have been docked with negative dock energy onto the target protein, it will be practical to give equal importance to all these protease inhibitor ligands**.**

## 3. Experimental

### 3.1. Instruments and apparatus

Melting points were determined by MEL-TEMP II melting point apparatus in open glass capillaries. The IR spectra were recorded as potassium bromide (KBr) discs on a Perkin-Elemer FT-IR (Fourier-Transform Infrared Spectroscopy), Faculty of Science, Alexandria University. The NMR spectra were carried out at ambient temperature (~25 °C) on a (JEOL) 500 MHz spectrophotometer using tetramethylsilane (TMS) as an internal standard, NMR Unit, Faculty of Science, Mansoura University. Elemental analyses were analyzed at the Regional Center for Mycology and Biotechnology, Al-Azhar University, Cairo, Egypt.

### 3.2. Docking program

Molecular docking simulations were performed to achieve the mode of interaction of prepared piperazines with the binding pocket of SARS-CoV-2 protease. The newly released crystal structure of SARS-CoV-2 main protease as a receptor was retrieved from protein data bank (www.rcsb.org) with PDB ID: 6M03 [50]. Software version 2015.10 of Molecular Operating Environment (MOE)

**Table 4**
Docking results of **3–11** docked into SARS-CoV-2 protease enzyme.

| Lig. | S (kcal/mol) | Type of interaction | Distance (A°) | Energy of each interaction (kcal/mol) |
|---|---|---|---|---|
| **3a** | −5.6962128 | H-acceptor (HIS 163) | 4.15 | −1.0 |
| | | H-acceptor (ASN 142) | 3.95 | −1.3 |
| | | H-acceptor (GLY 143) | 4.00 | −3.8 |
| **3b** | −5.8675022 | H-acceptor (ASN 142) | 3.72 | −1.2 |
| | | H-acceptor (GLY 143) | 4.00 | −1.3 |
| | | H-acceptor (SER 144) | 4.22 | −1.0 |
| **4** | −5.4194527 | H-donor (GLU 166) | 3.01 | −1.6 |
| | | H-donor (MET 165) | 3.46 | −1.5 |
| | | H-acceptor (ASN 142) | 3.81 | −1.8 |
| | | H-acceptor (GLY 143) | 4.00 | −3.4 |
| **8** | −6.8704705 | H-acceptor (THR 26) | 3.72 | −1.9 |
| | | H-acceptor (GLN 189) | 3.40 | −0.7 |
| | | H-acceptor (ASN 142) | 3.79 | −1.5 |
| | | H-acceptor (GLY 143) | 3.51 | −4.4 |
| **10** | −6.8147421 | H-acceptor (HIS 163) | 3.28 | −1.6 |
| | | H-pi (HIS 41) | 3.93 | −1.0 |
| | | pi-H (THR 25) | 3.76 | −0.8 |
| **9** | −5.8473911 | H-donor (CYS 145) | 3.54 | −0.9 |
| **5** | −5.7646523 | H-donor (GLU 166) | 3.10 | −0.6 |
| | | H-donor (GLU 166) | 3.33 | −2.4 |
| | | H-donor (ARG 188) | 4.17 | −0.8 |
| **6a** | −6.3332052 | H-acceptor (GLU 166) | 3.23 | −0.9 |
| **6b** | −6.6767573 | H-donor (GLN 189) | 3.33 | −0.7 |
| | | H-acceptor (GLU 166) | 3.28 | −1.1 |
| **7** | −6.5700703 | H-donor (PHE 140) | 3.53 | −0.7 |
| | | pi-H (MET 49) | 4.74 | −0.7 |
| **11** | −5.43680048 | H-donor (CYS 145) | 3.20 | −1.0 |
| | | H-acceptor (ASN 142) | 3.47 | −0.8 |
| | | H-acceptor (GLY 143) | 3.39 | −0.6 |
| | | H-acceptor (GLU 166) | 3.12 | −3.0 |
| **12** | −4.8515186 | pi-H (Meth 165) | 3.97 | −1.0 |

was used to prepare the input files and analyzing the result. All water molecules, ligands and ions were removed from pdb file for the preparation of protein input file. The active site was selected utilizing 'Site Finder' MOE 2015.10 feature. Prior to docking, the piperazines structures were subjected to energy minimization and geometry optimization before docking. Docking simulations were conducted several times with various fitting protocols to observe the best molecular interactions and free binding energies. All docking results were sorted by scoring binding energy.

### 3.3. General method for synthesis of piperazines 2–12

#### 3.3.1. Bis(triethylammonium) piperazine-1,4-bis(dithiocarbomate) 2

A mixture of piperazine (2 g, 0.023 mol) and triethylamine (12.8 mL) dissolved in THF (10 mL) in an ice bath was received carbon disulfide (4.25 mL) drop wise with constant stirring. After complete addition of carbon disulfide, the reaction was stirred at room temperature for 18 h. Pale yellow precipitate was formed filtered, washed 4 times with hexane:ethylacetate (5:95), 8.9 g (87%) yield; m.p.215–220 °C. [28]

#### 3.3.2. General procedure of dialkylpiperazine-1,4-bis(carbodithioate) 3a,b

Alkyl iodide [ethyl iodide (2.31 mL) or methyl iodide (1.23 mL)] was drop wisely added to a stirred solution of piperazine-1,4-bis(dithiocarbomate salt) **2** (4 gm, 0.009 mol) in water (25 mL) under an ice cooled condition. The reaction mixture was stirred overnight at room temperature. The separated solid was filtered off then crystallized from ethanol.

#### 3.3.3. Dimethyl piperazine-1,4-bis(carbodithioate) 3a [51]

Pale yellow crystals, 2.33 g (87%) yield; m.p. 180 °C. IR $cm^{-1}$(KBr): 2992 ($sp^3$C-H**),** 1458 (N–CSS, dithiocarbamate) and 1158 (-C-N) $cm^{-1}$. $^1$H NMR (400 MHz, $CDCl_3$): $\delta$ ppm: 4.16 (s, 8H, piperazine-4$CH_2$) and 2.67 (s, 6H, 2$CH_3$) ppm. $^{13}$C APT NMR (101 MHz, $CDCl_3$): $\delta$ 199.22, 46.24 and 20.11 ppm. $C_8H_{14}N_2S_4$ requires: C: 36.05; H: 5.30; N: 10.51%, found: C: 36.47; H: 5.54; N: 10.27%.

#### 3.3.4. Diethyl piperazine-1,4-bis-carbodithioate 3b [51,52]

White crystals, 2.26 g (97%) yield; m.p. 125 °C. IR $cm^{-1}$ (KBr): 2997 ($sp^3$C-H**),** 1463 (N–CSS, dithiocarbamate) and 1159 (C–N) $cm^{-1}$. $^1$H NMR (500 MHz, $CDCl_3$) $\delta$ ppm: 3.34 (s, 8H, piperazine-4$CH_2$), 3.23 (q, $J$ = 7.4 Hz, 4H, 2S-$CH_2$) and 1.26 (t, $J$ = 7.3 Hz, 6H, 2$CH_3$) ppm. $^{13}$C APT NMR (126 MHz, $CDCl_3$): $\delta$ 195.70, 47.63, 30.51 and 13.54 ppm. $C_{10}H_{18}N_2S_4$ requires: C: 40.77; H: 6.17; N: 9.51%, found: C: 41.01; H: 6.25; N: 9.21%.

#### 3.3.5. Piperazine-1,4-bis(carbothiohydrazide) 4 [53]

A mixture of dimethyl piperazine-1,4-bis-carbodithioate **3a** (4 gm, 0.013 mol) and hydrazine hydrate (98%) (19.8 ml) in ethanol (25 mL) was refluxed for 30 h. On cooling the reaction mixture, the solid which separated was filtered, washed, dried and no need to extra purification. gray powder, 2.23 g (70%) yield; m.p. 218–220 °C. IR $cm^{-1}$ (KBr): 3267 ($NH_2$**),** 3088 (NH), 2927 ($sp^3$ -C-H), 1159 (C–N), 1645 (-N-*C* = *S*, thioamide) and 1159 (C–N). $^1$H NMR (500 MHz, DMSO–$d_6$) $\delta$ ppm: 9.07 (br.s, 2H, 2NH, $D_2O$ exchangeable), 4.87 (Br.s, 4H, 2$NH_2$, $D_2O$ exchangeable) and 3.78 (s, 8H, piperazine-4$CH_2$) ppm. $^{13}$C APT NMR (126 MHz, DMSO–$d_6$): 182.47 and 46.11 ppm. $C_6H_{14}N_6S_4$ requires: C: 30.74, H: 6.03, N, 35.86%, found: C: 31.45, H: 6.29, N, 35.46%.

#### 3.3.6. 5,5′-(Piperazin-1,4-diyl)bis(1,3,4-thiadiazole-2-thiol) 5

The mixture of piperazine-1,4-bis(carbothiohydrazide) **4** (5 gm, 0.021 mol), dimethylformamide (12 mL) and carbon disulphide (10 mL) were refluxed for 4 h. The mixture was poured into ice water and the precipitated product was filtered then crystallized from ethanol to yield light yellow powder, 6.61 g (97%) yield; m.p. 290–300 °C. IR (KBr): 2909 ($sp^3$-C-H), 2580 (SH**),** 1554 (*C* = *N*), 1172 (C–N) and 718 (C-S) $cm^{-1}$. $^1$H NMR (500 MHz,

DMSO–$d_6$): $\delta$ 13.65 (Br.s, 2H, 2SH, $D_2O$ exchangeable) and 3.39 (s, 8H, piperazine-4$CH_2$) ppm. $^{13}$C APT NMR (126 MHz, DMSO–$d_6$): $\delta$ 181.57, 163.20 and 46.86 ppm. $C_8H_{10}N_6S_4$ requires: C: 30.16; H: 3.17; N: 26.39%, found: C: 30.43; H: 3.25; N: 26.57%.

### 3.3.7. General procedure of 1,4-bis(5-(alkylthio)−1,3,4-thiadiazol-2-yl)piperazine 6a,b

Alkyl iodide [methyl iodide (12.5 mL) or ethyl iodide (12.5 mL)] was drop wise added to stirring mixture of 5,5′-(piperazin-1,4-diyl)bis(1,3,4-thiadiazole-2-thiol) **8** (5 gm, 0.015 mol) and KOH (1.5 gm, 0.026 mol) in ethanol (35 mL). The mixture was further stirred for 4 h then poured into ice water and the precipitated formed washed with water, dried and crystalized from ethanol.

### 3.3.8. 1,4-Bis(5-(methylthio)−1,3,4-thiadiazol-2-yl)piperazine 6a

Pale white powder, 3.34 g (61%) yield; m.p. 215 °C. IR cm$^{-1}$ (KBr): 2951 (sp$^3$C-H), 1517 (*C = N*), 1107 (C–N), and 742 (C-S). $^1$H NMR (400 MHz, $CDCl_3$) $\delta$ ppm: 3.64 (s, 8H, piperazine-4$CH_2$) and 2.68 (s, 6H, 2$CH_3$) ppm. $^{13}$C APT NMR (101 MHz, $CDCl_3$): 171.95, 155.95, 49.08 and 16.83 ppm. $C_{10}H_{14}N_6S_4$ requires: C: 34.65; H: 4.08; N: 24.25%, found: C: 34.35; H: 4.27; N: 24.64%.

### 3.3.9. 1,4-Bis(5-(ethylthio)−1,3,4-thiadiazol-2-yl)piperazine 6b

Pale white crystalline powder, 3.38 g (57%) yield; m.p.220 °C. IR cm$^{-1}$ (KBr): 2983 (sp$^3$C-H), 1517 (*C = N*), 1105 (C–N), and 742 (C-S). $^1$H NMR (500 MHz, $CDCl_3$): $\delta$ ppm: 3.67 (s, 8H, piperazine-4$CH_2$), 3.17 (q, 4H, 2$CH_2$) and 1.41 (s, 6H, 2$CH_3$). $^{13}$C APT NMR

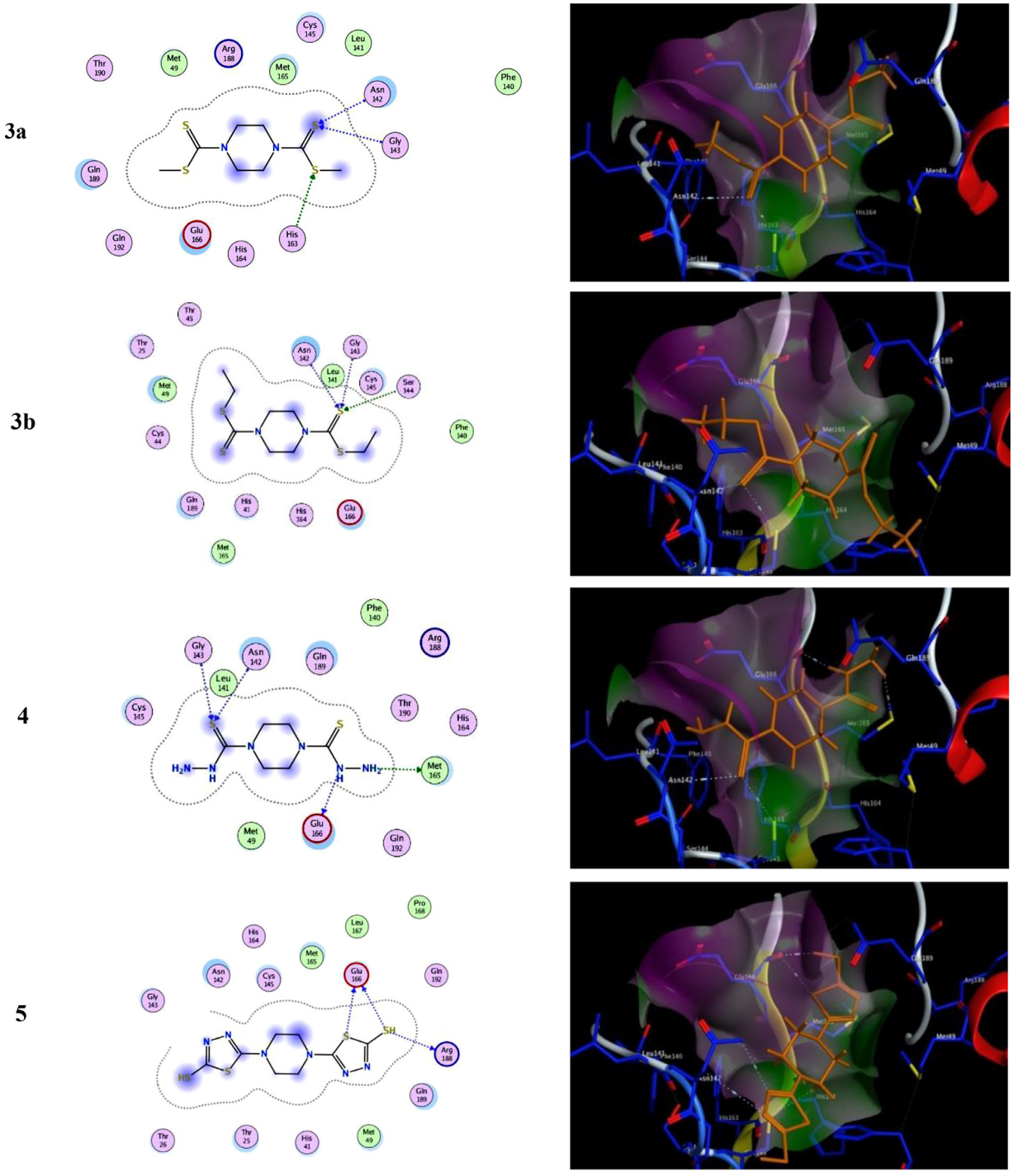


**Fig. 2.** 2D and 3D binding modes of **3–12** (orange tube) in protease active sites (PDB: 6M03 [50]).

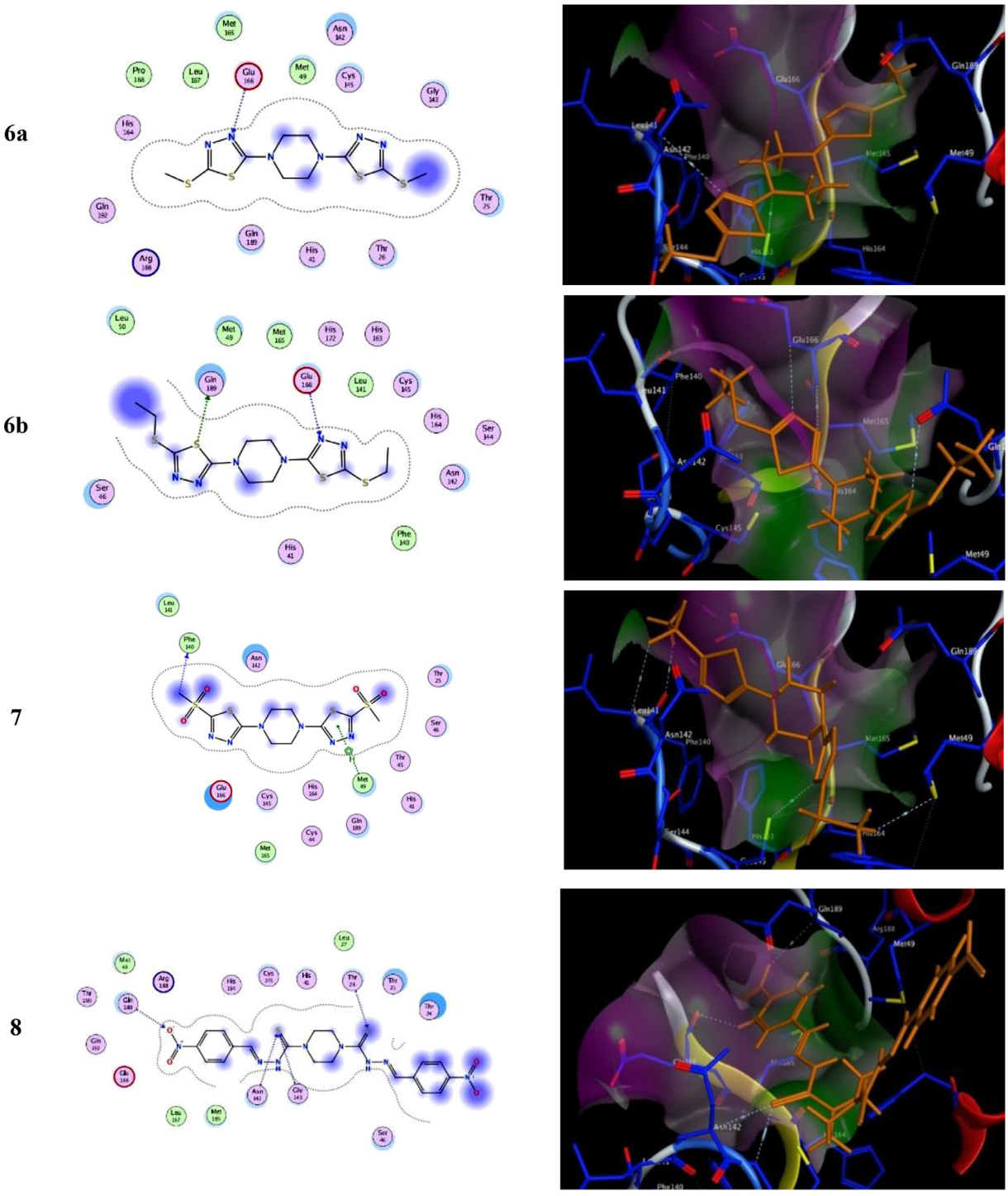


**Fig. 2.** Continued

(126 MHz, $CDCl_3$): $\delta$ 172.23, 154.61, 49.06, 29.32 and 14.95 ppm. $C_{12}H_{18}N_6S_4$ requires: C: 38.47; H: 4.85; N: 22.43%, found: C: 38.53; H: 4.52; N: 22.87%.

*3.3.10. 1,4-Bis(5-(methylsulfonyl)−1,3,4-thiadiazol-2-yl)piperazine 7*

The treatment of 1,4-bis(5-(methylthio)−1,3,4-thiadiazol-2-yl)piperazine **187a** (0.25 gm, 0.0007 mol) dissolved in ethanol (20 mL), with hydrogen peroxide (34%, 7 mL) was stirred at room temperature. After the completion of addition, the stirring was continuing overnight, then the excess of solvent was evaporated, cooled, filtered and then crystalizes from ethanol to give white powder, 0.14 g (48%) yield; m.p. 250 °C. IR $cm^{-1}$ (KBr): 2962 ($sp^3$C-H**),** 1516 (*C = N*), 1103 (C–N), 767 (C-S) and 1308–1152 ($SO_2$, asymmetry and Symmetry). $^1$H NMR (400 MHz, DMSO–$d_6$), $\delta$ ppm: 3.77 (s, 8H, piperazine-4$CH_2$) and 3.04 (s, 6H, 2$CH_3$) ppm. $^{13}$C APT NMR (125 MHz: DMSO–*d6*): 184.46, 161.90, 48.85 and 42.84. $C_{10}H_{14}N_6O_4S_4$ requires: C: 29.25; H: 3.44, N: 20.47% found: C: 29.12; H: 3.27, N: 20.32%.

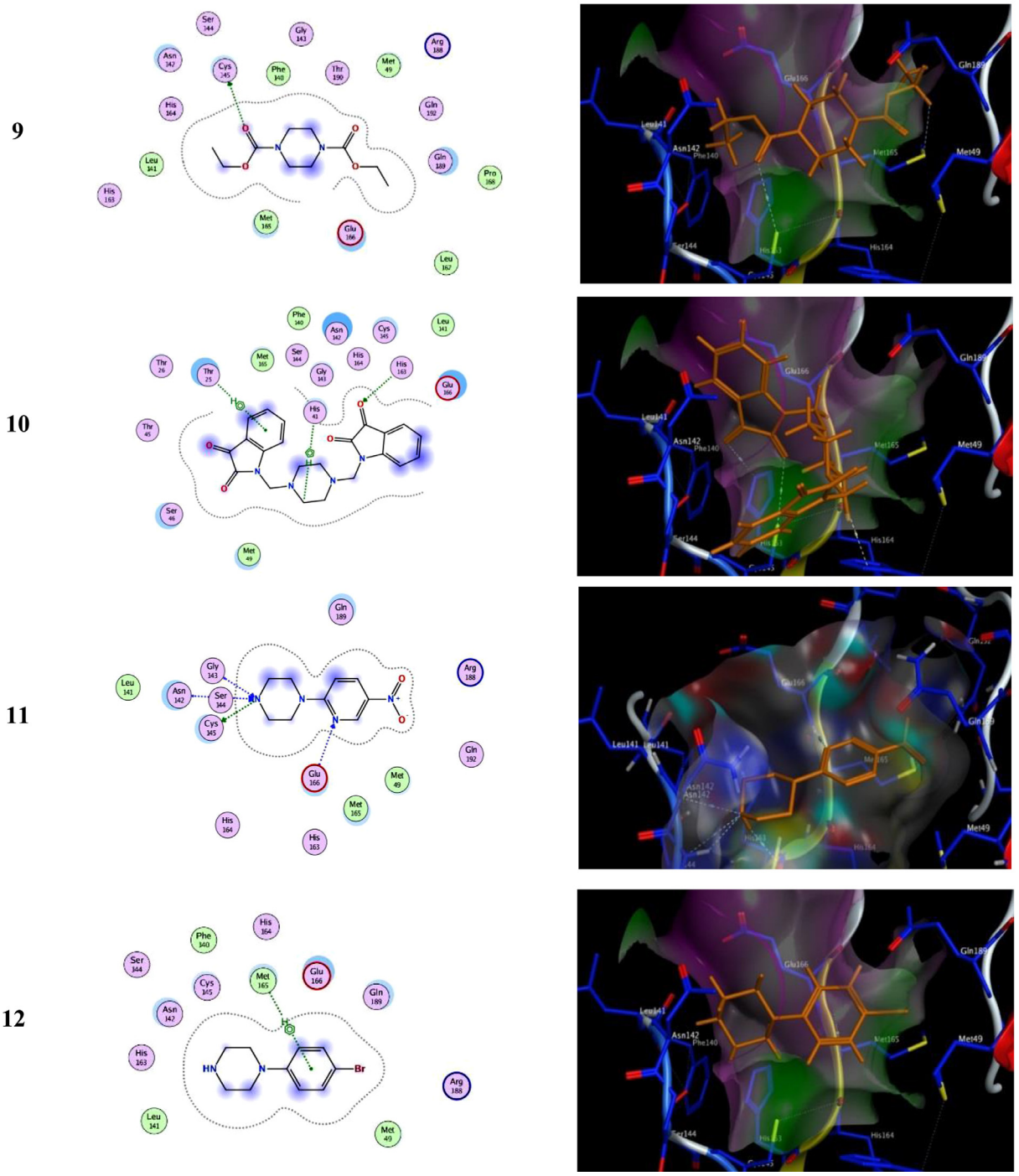


**Fig. 2.** Continued

*3.3.11. 1,4-Bis(4-nitrobenzylidene)piperazine-1,4-bis(carbothiohydrazide) 8 [54]*

Piperazine-1,4-bis(carbothiohydrazide) **4** (0.5 gm, 0.00213 mol) dissolved in acetic acid (10 mL) was treated with *p*-nitrobenzaldehyde (0.64 gm, 0.00213 mol) and the mixture was refluxed for 25 h. The product precipitated while hot was filtered and dried to give dark red powder, 0.56 g (52%) yield; m.p. 175 °C. IR (KBr): 3440 (N–H), 2990 ($sp^3$ -C-H), 1594 (*S* = *C*–N-, thioamide), 1106 (C–N) and 1519–1344 ($NO_2$, Asymmetry and Symmetry) $cm^{-1}$. $^1H$ NMR (500 MHz, DMSO–$d_6$): $\delta$ 10.16 (Br.s, 2H, 2NH, $D_2O$ exchangeable), 8.86 (s, 2H, 2N=CH), 8.25 (m, 8H, Ar-H) and 4.09 (s, 8H, piperazine-$4CH_2$) ppm. $^{13}C$ APT NMR (126 MHz, DMSO–$d_6$): $\delta$ 192.40, 147.89, 140.08, 130.68, 129.62, 124.32 and 49.05 ppm. $C_{20}H_{20}N_8O_4S_4$ requires: C: 47.98; H: 4.03, N: 22.38%, found: C: 48.25; H: 4.12, N: 22.12%.

*3.3.12. Diethyl piperazine-1,4-dicarboxylate 9*

A solution of piperazine **1** (5 gm, 0.058 mol) in dichloromethane (75 mL) was cooled to 0 °C then triethylamine (24 mL) was added. The reaction was proceeded by drop wise addition of a solution of ethyl chloroformate (11 mL) in dichloromethane (35 mL). After stirring overnight at room temperature, the mixture was filtered and subject to extract with 3 M

HCl. The organic layer was dried over sodium sulfate then evaporated to give diethyl piperazine-1,4-dicarboxylate. White solid, 7.23 g (54%) yield; m.p. 45–47 °C. IR $cm^{-1}$ (KBr): 2994 ($sp^3$C-H), 1708 (N–OCO, carbamate) and 1109 (-C-N). $^1$H NMR (500 MHz, $CDCl_3$): $\delta$ ppm: 4.13 (q, 4H, $2CH_2$), 3.42 (s, 8H, piperazine-$4CH_2$) and 1.24 (t, 6H, $2CH_3$). $^{13}$C APT NMR (101 MHz, $CDCl_3$): $\delta$ 155.37, 61.58, 43.02 and 14.68. $C_{10}H_{18}N_2O_4$ requires: C: 52.14; H: 7.89, N, 12.16%, found: C: 52.47; H: 8.02, N: 12.47%.

### 3.3.13. 1,1′-(Piperazin-1,4-diylbis(methylene))bis(indoline-2,3–dione) 10

Piperazine **1** (0.5 gm, 0.0058 mol) in ethanol was added drop wise with shaken to a solution of isatin, (1.7 gm, 0.011 mol) in (10 mL) and formaldehyde 40% (6 mL).in ethanol. The mixture was stirred at room temperature for overnight and the reaction progress was detected by TLC in hexane:ethylacetate (2:8). After reaction completion, the precipitate was filtrated and dried. Dark orange, 2.20 g (93%) yield; m.p. 262 - 265 °C. IR) $cm^{-1}$ (KBr): 3025 ($sp^2$ =C–H), 2954 ($sp^3$ -C-H), 1738 (*C = O*, ketone), 1612 (*C = O*, amide) and 1135 (C–N. $^1$H NMR (500 MHz, DMSO–$d_6$): $\delta$ ppm 7.63 (t, $J$ = 7.7, 2H, H-6 and H-6′), 7.53 (d, $J$ = 7.4 Hz, 2H, H-7 and H-7′), 7.24 (d, $J$ = 8.0 Hz, 2H, H-4 and H-4′), 7.12 (t, $J$ = 7.5 Hz, 2H, H-5 and H-5′), 4.38 (s, 4H, $2CH_2$) and 3.34 (s, 8H, piperazine-$4CH_2$). $^{13}$C APT NMR (126 MHz, DMSO–$d_6$): $\delta$ 183.20, 158.99, 151.59, 137.94, 124.21, 123.22, 117.54, 112.02, 61.53 and 49.82 ppm. $C_{22}H_{20}N_4O_4$ requires: C: 65.32; H: 4.99; N: 13.85%, found: C: 65.52; H: 4.76; N: 13.91%.

### 3.3.14. 1-(5-Nitropyridin-2-yl)piperazine 11

A mixture of 2–chloro-5-nitropyridine **11** (2.69 gm, 0.016 mol), NaH and piperazine **1** (3.11 gm, 0.0036 mol) in 1,4-dioxane (20 mL) was refluxed for 24 h. The progress of reaction was checked with the help of TLC. After completion of reaction, the mixture was poured into ice water. The product which separated was filtered and washed with water. Dark yellow crystalline, 1.25 g (51%) yield; m.p. 126 - 130 °C. IR $cm^{-1}$ (KBr): 3340 (N–H), 3037 ($sp^2$ =C–H), 2922 ($sp^3$ C–H), 1128 (C–N) and 1597- 1321 ($NO_2$, asymmetry and symmetry). $^1$H NMR $\delta$ ppm. (500 MHz, $CDCl_3$): $\delta$ ppm 9.03 (d, $J$ = 2.7 Hz, 1H, H-6), 8.19 (dd, $J$ = 9.4, 2.8 Hz, 1H, H-4), 6.55 (d, $J$ = 9.6 Hz, 1H, H-3), 3.74 (t, $J$ = 5.0 Hz, 2H, piperazine-$2CH_2$) and 2.97 (t, $J$ = 5.0 Hz, 2H, piperazine-$2CH_2$). $^{13}$C APT NMR (101 MHz, $CDCl_3$): $\delta$ 160.61, 146.64, 135.00, 133.11, 104.59, 46.16 and 46.00 ppm. $C_9H_{12}N_4O_2$ requires: C: 51.90; H: 5.81, N: 26.90%, found: C: 51.76; H: 5.76, N: 26.57%.

### 3.3.15. Bis(2-chloroethyl)amine hydrochloride

Thionyl chloride (65 mL) in chloroform (65 mL) was added drop wise with constant stirring to a solution of diethanolamine (25 mL) in chloroform (75 mL), (addition during 1 h). The mixture was then refluxed for 30 min with stirring. On cooling the solution to room temperature, a white solid product was separated, filtered and washed with chloroform and ether to give white powder, 43 g (92%) yield; m.p.110–120 °C. [38]

### 3.3.16. 1-(4-Bromophenyl)piperazine 12

A mixture of 4-bromoaniline (3 gm, 0.017 mol) and bis($\beta$-chloroethyl)amine hydrochloride (3.11 gm, 0.017 mol) in 1-propanol (20 mL) was refluxed for 24 h. The reaction mixture was cooled and anhydrous $K_2CO_3$ (2.32 gm, 0.016 mol) was added then continue refluxing for another 48 h. The progress of reaction was checked with the help of TLC. After completion of reaction, the mixture was filtered while hot and the filtrate was cooled. The precipitate separated was filtered and washed successively with 1-propanol and ether to obtain pale yellow crystalline powder 3.12 g (74%) yield m.p: 91–94 °C. IR $cm^{-1}$ (KBr): 3404 (N–H), 2935 ($sp^3$ -C-H) and 1057 (C–N),. $^1$H NMR (500 MHz, DMSO–$d_6$) $\delta$ ppm: 9.37 (Br.s, 1H, NH, $D_2O$ exchangeable), 7.38 (d, $J$ = 8.9 Hz, 2H, Ar-H), 6.93 (d, $J$ = 9.0 Hz, 2H, Ar-H), 3.35 (t, $J$ = 5.9 Hz, 4H, piperazine-$2CH_2$) and 3.16 (t, $J$ = 5.6 Hz, 4H, $2CH_2$-piperazine) ppm. $^{13}$C APT NMR (126 MHz, DMSO–$d_6$): 149.31, 131.77, 118.06, 111.31, 45.19 and 42.43. $C_{10}H_{13}BrN_2$ requires: C, 49.80; H 5.44, N: 11.61%, found: C, 49.67; H 5.21, N, 11.35%.

## Credit author statement

**Author Contributions: Samer K. Elsadany, Ezzat A. Hamed, Mohamed Elatawy** and **Alaa Z. Omar** designed the research; **Alaa Z. Omar, Mohamed Elatawy** and **Tawfik M. Mosa** performed the experimental work and analyzed the data; **Samer K. Elsadany, Ezzat A. Hamed, Mohamed Elatawy** and **Alaa Z. Omar** wrote the manuscript; **Ezzat A. Hamed, Mohamed Elatawy** and **Alaa Z. Omar** revised the manuscript. All the authors discussed, edited, and approved the final version.

## Declaration of Competing Interest

The authors declare that they have no known competing financial interests or personal relationships that could have appeared to influence the work reported in this paper.

## Supplementary materials

Supplementary material associated with this article can be found, in the online version, at doi:10.1016/j.molstruc.2021.131020.

## References

[1] S.A. Amin, T. Jha, Fight against novel coronavirus: a perspective of medicinal chemists, Eur. J. Med. Chem. (2020) 112559.
[2] C. Liang, L. Tian, Y. Liu, N. Hui, G. Qiao, H. Li, Z. Shi, Y. Tang, D. Zhang, X. Xie, A promising antiviral candidate drug for the COVID-19 pandemic: a mini-review of remdesivir, Eur. J. Med. Chem. (2020) 112527.
[3] L. Zhang, D. Lin, X. Sun, U. Curth, C. Drosten, L. Sauerhering, S. Becker, K. Rox, R. Hilgenfeld, Crystal structure of SARS-CoV-2 main protease provides a basis for design of improved $\alpha$-ketoamide inhibitors, Science 368 (2020) 409–412.
[4] M.J. Akhtar, COVID19 inhibitors: a prospective therapeutics, Bioorg. Chem 101 (2020) 104027.
[5] Q. Tan, L. Duan, Y. Ma, F. Wu, Q. Huang, K. Mao, W. Xiao, H. Xia, S. Zhang, E. Zhou, Is oseltamivir suitable for fighting against COVID-19: in silico assessment, in vitro and retrospective study, Bioorg. Chem (2020) 104257.
[6] Faheem, B. Karan Kumar, K. Venkata Gowri Chandra Sekhar, S. Kunjiappan, J. Jamalis, R. Balaña-Fouce, B.L. Tekwani, M. Sankaranarayanan, Druggable targets of SARS-CoV-2 and treatment opportunities for COVID-19, Bioorg. Chem (2020) 104269.
[7] D. Mothay, K. Ramesh, Binding site analysis of potential protease inhibitors of COVID-19 using AutoDock, Virusdisease (2020) 1.
[8] S.-.Q. Deng, H.-.J. Peng, Characteristics of and public health responses to the coronavirus disease 2019 outbreak in China, J. Clin. Med. 9 (2020) 575.
[9] D.L. Heymann, N. Shindo, COVID-19: what is next for public health? The Lancet 395 (2020) 542–545 https://www.worldometers.info/coronavirus/.
[10] Z. Song, Y. Xu, L. Bao, L. Zhang, P. Yu, Y. Qu, H. Zhu, W. Zhao, Y. Han, C. Qin, From SARS to MERS, thrusting coronaviruses into the spotlight, Viruses 11 (2019) 59.
[11] K. Anand, J. Ziebuhr, P. Wadhwani, J.R. Mesters, R. Hilgenfeld, Coronavirus main proteinase (3CLpro) structure: basis for design of anti-SARS drugs, Science 300 (2003) 1763–1767.
[12] P.C. Woo, Y. Huang, S.K. Lau, K.-.Y. Yuen, Coronavirus genomics and bioinformatics analysis, Viruses 2 (2010) 1804–1820.
[13] J. Ziebuhr, Molecular biology of severe acute respiratory syndrome coronavirus, Curr. Opin. Microbiol. 7 (2004) 412–419.
[14] G.E.A. Aynelabro, The species Severe acute respiratory syndrome-related coronavirus: classifying 2019-nCoV and naming it SARS-CoV-2, Nat. Microbiol. 5 (2020) 536.
[15] L. Wang, B.-.B. Bao, G.-.Q. Song, C. Chen, X.-.M. Zhang, W. Lu, Z. Wang, Y. Cai, S. Li, S. Fu, Discovery of unsymmetrical aromatic disulfides as novel inhibitors of SARS-CoV main protease: chemical synthesis, biological evaluation, molecular docking and 3D-QSAR study, Eur. J. Med. Chem. 137 (2017) 450–461.
[16] D.S. Goodsell, A.J. Olson, Automated docking of substrates to proteins by simulated annealing, Proteins 8 (1990) 195–202.
[17] Y. Chen, Q. Liu, D. Guo, Emerging coronaviruses: genome structure, replication, and pathogenesis, J. Med. Virol. 92 (2020) 418–423.
[18] J. Ziebuhr, E.J. Snijder, A.E. Gorbalenya, Virus-encoded proteinases and proteolytic processing in the Nidovirales, J. Gen. Virol. 81 (2000) 853–879.

[19] P.S. Masters, The molecular biology of coronaviruses, Adv. Virus Res. 66 (2006) 193–292.
[20] J. Ziebuhr, G. Heusipp, S.G. Siddell, Biosynthesis, purification, and characterization of the human coronavirus 229E 3C-like proteinase, J. Virol. 71 (1997) 3992–3997.
[21] R.A. Khailany, M. Safdar, M. Ozaslan, Genomic characterization of a novel SARS-CoV-2, Gene Rep (2020) 100682.
[22] F. Wang, C. Chen, W. Tan, K. Yang, H. Yang, Structure of main protease from human coronavirus NL63: insights for wide spectrum anti-coronavirus drug design, Sci. Rep. 6 (2016) 22677.
[23] R.M. Gulick, X. Joan Hu, S.A. Fiscus, C.V. Fletcher, R. Haubrich, H. Cheng, E. Acosta, S.W. Lagakos, R. Swanstrom, W. Freimutn, Randomized study of saquinavir with ritonavir or nelfinavir together with delavirdine, adefovir, or both in human immunodeficiency virus—infected adults with virologic failure on indinavir: AIDS clinical trials group study 359, J. Infect. Dis. 182 (2000) 1375–1384.
[24] L.J. Scott, C.M. Perry, Delavirdine, Drugs 60 (2000) 1411–1444.
[25] J. Droste, C. Verweij-van Wissen, D. Burger, Simultaneous determination of the HIV drugs indinavir, amprenavir, saquinavir, ritonavir, lopinavir, nelfinavir, the nelfinavir hydroxymetabolite M8, and nevirapine in human plasma by reversed-phase high-performance liquid chromatography, Ther. Drug Monit. 25 (2003) 393–399.
[26] H. Zhou, M.A. McGowan, K. Lipford, M. Christopher, X. Fradera, D. Witter, C.A. Lesburg, C. Li, J.L. Methot, J. Lampe, Discovery and optimization of heteroaryl piperazines as potent and selective PI3K$\delta$ inhibitors, Bioorg. Med. Chem. Lett. 30 (2020) 126715.
[27] Ranjbar-Karimi, R. and Poorfreidoni, A., Chemoselectivity of S and N Nucleophiles Toward Pentachloropyridine, 2017.
[28] G. Serban, O. Stanasel, E. Serban, S. Bota, 2-Amino-1, 3, 4-thiadiazole as a potential scaffold for promising antimicrobial agents, Drug Des., Devel. Ther. 12 (2018) 1545.
[29] J. Chen, C. Yi, S. Wang, S. Wu, S. Li, D. Hu, B. Song, Novel amide derivatives containing 1, 3, 4-thiadiazole moiety: design, synthesis, nematocidal and antibacterial activities, Bioorg. Med. Chem. Lett. 29 (2019) 1203–1210.
[30] Y. Li, J. Geng, Y. Liu, S. Yu, G. Zhao, Thiadiazole—a promising structure in medicinal chemistry, ChemMedChem 8 (2013) 27–41.
[31] C. Steeneck, C. Gege, O. Kinzel, M. Albers, G. Kleymann, T. Schlüter, A. Schulz, X. Xue, M.D. Cummings, A.M. Fourie, Discovery and optimization of new oxadiazole substituted thiazole ROR$\gamma$t inverse agonists through a bioisosteric amide replacement approach, Bioorg. Med. Chem. Lett. (2020) 127174.
[32] S.Y. Abbas, A.A. Farag, Y.A. Ammar, A.A. Atrees, A.F. Mohamed, A.A. El-Henawy, Synthesis, characterization, and antiviral activity of novel fluorinated isatin derivatives, Monatsh. Chem. 144 (2013) 1725–1733.
[33] P. Selvam, N. Murgesh, M. Chandramohan, E. De Clercq, E. Keyaerts, L. Vijgen, P. Maes, J. Neyts, M. Ranst, In vitro antiviral activity of some novel isatin derivatives against HCV and SARS-CoV viruses, Ind, J. Pharm. Sci. 70 (2008) 91.
[34] F.A. Khan, A. Maalik, Advances in pharmacology of isatin and its derivatives: a review, Trop. J. Pharm. Res. 14 (2015) 1937–1942.
[35] S.N. Pandeya, S. Smitha, M. Jyoti, S.K. Sridhar, Biological activities of isatin and its derivatives, Acta Pharm 55 (2005) 27–46.
[36] S.S. Daher, K.P. Franklin, T. Scherzi, P.M. Dunman, R.B. Andrade, Synthesis and biological evaluation of semi-synthetic albocycline analogs, Bioorg. Med. Chem. Lett. (2020) 127509.
[37] V.K. Jain, B. Jain, U.K. Sharma, D. Saha, Synthesis, characterization and antimicrobial screening of some 4-substituted-1-(4-substituted phenyl) piperazine derivatives, Int. J. Curr. Pharm. Res. 3 (2011) 66–70.
[38] T. B Fernandes, M. CF Segretti, M. C Polli, R. Parise-Filho, Analysis of the applicability and use of Lipinskis rule for central nervous system drugs, Lett. Drug Des. Discov. 13 (2016) 999–1006.
[39] N. Boutard, A. Białas, A. Sabiniarz, P. Guzik, K. Banaszak, A. Biela, M. Bień, A. Buda, B. Bugaj, E. Cieluch, Synthesis of amide and sulfonamide substituted N-aryl 6-aminoquinoxalines as PFKFB3 inhibitors with improved physicochemical properties, Bioorg. Med. Chem. Lett. 29 (2019) 646–653.
[40] S. Chitti, S. Singireddi, P.S.K. Reddy, P. Trivedi, Y. Bobde, C. Kumar, K. Rangan, B. Ghosh, K.V.G.C. Sekhar, Design, synthesis and biological evaluation of 2-(3, 4-dimethoxyphenyl)-6 (1, 2, 3, 6-tetrahydropyridin-4-yl) imidazo [1, 2-a] pyridine analogues as antiproliferative agents, Bioorg. Med. Chem. Lett. 29 (2019) 2551–2558.
[41] S. Khan, S. Kumar, A. Maqsood, Virtual screening of molecular properties and bioactivity score of boswellic acid derivatives in search of potent anti-inflammatory lead molecule, Intern, Int. J. Interdiscip. Multidiscip. Stud. 1 (2013) 8–12.
[42] S. Rajasekaran, G. Rao, Molecular Properties and Bio-Activity Score of 2 {[2-(4-chlorophenyl)-4-oxoquinazolin-3 (4H)-yl] amino}-N-(substitutedphenyl) Acetamides, J. Pharm. Res. 16 (2017) 95–98.
[43] A. Joshi, R. Kumar, A. Sharma, Molecular docking studies, bioactivity score prediction, drug likeness analysis of GSK-3 $\beta$ inhibitors: a target protein involved in Alzheimer's disease, Biosci. Biotechnol. Res. Asia 15 (2018) 455–467.
[44] A. Šmelcerović, K. Tomović, Ž. Šmelcerović, Ž. Petronijević, G. Kocić, T. Tomašič, Ž. Jakopin, M. Anderluh, Xanthine oxidase inhibitors beyond allopurinol and febuxostat; an overview and selection of potential leads based on in silico calculated physico-chemical properties, predicted pharmacokinetics and toxicity, Eur. J. Med. Chem. 135 (2017) 491–516.
[45] M.A.d. Brito, Pharmacokinetic study with computational tools in the medicinal chemistry course, Eur. J. Med. Chem. 47 (2011) 797–805.
[46] E. Stingaci, M. Zveaghinteva, S. Pogrebnoi, L. Lupascu, V. Valica, L. Uncu, A. Smetanscaia, M. Drumea, A. Petrou, A. Ciric, New vinyl-1, 2, 4-triazole derivatives as antimicrobial agents: synthesis, biological evaluation and molecular docking studies, Bioorg. Med. Chem. Lett. 30 (2020) 127368.
[47] B. Tan, X. Zhang, X. Quan, G. Zheng, X. Li, L. Zhao, W. Li, B. Li, Design, synthesis and biological activity evaluation of novel 4-((1-cyclopropyl-3-(tetrahydro-2H-pyran-4-yl)-1H-pyrazol-4-yl) oxy) pyridine-2-yl) amino derivatives as potent transforming growth factor-$\beta$ (TGF-$\beta$) type I receptor inhibitors, Bioorg. Med. Chem. Lett. (2020) 127339.
[48] S. Ullrich, C. Nitsche, The SARS-CoV-2 main protease as drug target, Bioorg. Med. Chem. Lett. 30 (2020) 127377.
[49] X. Liu, B. Zhang, Z. Jin, H. Yang, Z. Rao, The Crystal Structure of COVID-19 Main Protease in Complex with an Inhibitor N3, Protein DataBank, 2020.
[50] E. Zhang, M.-.M. Wang, S.-.C. Huang, S.-.M. Xu, D.-.Y. Cui, Y.-.L. Bo, P.-.Y. Bai, Y.-.G. Hua, C.-.L. Xiao, S. Qin, NOTA analogue: a first dithiocarbamate inhibitor of metallo-$\beta$-lactamases, Bioorg. Med. Chem. Lett. 28 (2018) 214–221.
[51] S. Braverman, M. Cherkinsky, M. Birsa, Carbon dioxide, carbonyl sulfide, carbon disulfide, isocyanates, isothiocyanates, carbodiimides, and their selenium, tellurium, and phosphorus analogues, ChemInform 36 (2005) no-no.
[52] R. Chandra, O. Pandey, S. Sengupta, Organophosphorus derivatives containing piperazine dithiosemicarbazones as chemotherapeutants against fungal pathogens of sugarcane, J. Agric. Food Chem. 53 (2005) 2181–2184.
[53] O. Pandey, S. Sengupta, M. Mishra, C. Tripathi, Synthesis, spectral and antibacterial studies of binuclear titanium (IV)/zirconium (IV) complexes of piperazine dithiosemicarbazones, Bioinorg. Chem. Appl. 1 (2003) 35–44.